H4K20 methylation regulates quiescence and chromatin compaction

Adam G. Everttsa, Amity L. Manningb, Xin Wanga, Nicholas J. Dysonb, Benjamin A. Garciac, and Hilary A. Collerd

aDepartment of Molecular Biology, Princeton University, Princeton, NJ 08544; bMassachusetts General Hospital Cancer Center, Harvard Medical School, Charlestown, MA 02129; cDepartment of Biochemistry and Biophysics, University of Pennsylvania, Philadelphia, PA 19104; dDepartment of Molecular, Cell and Developmental Biology, University of California, Los Angeles, and Department of Biological Chemistry, David Geffen School of Medicine, Los Angeles, CA 90095

ABSTRACT **The transition between proliferation and quiescence is frequently associated with changes in gene expression, extent of chromatin compaction, and histone modifications, but whether changes in chromatin state actually regulate cell cycle exit with quiescence is unclear. We find that primary human fibroblasts induced into quiescence exhibit tighter chromatin compaction. Mass spectrometry analysis of histone modifications reveals that H4K20me2 and H4K20me3 increase in quiescence and other histone modifications are present at similar levels in proliferating and quiescent cells. Analysis of cells in S, G_2/M, and G_1 phases shows that H4K20me1 increases after S phase and is converted to H4K20me2 and H4K20me3 in quiescence. Knockdown of the enzyme that creates H4K20me3 results in an increased fraction of cells in S phase, a defect in exiting the cell cycle, and decreased chromatin compaction. Overexpression of Suv4-20h1, the enzyme that creates H4K20me2 from H4K20me1, results in G_2 arrest, consistent with a role for H4K20me1 in mitosis. The results suggest that the same lysine on H4K20 may, in its different methylation states, facilitate mitotic functions in M phase and promote chromatin compaction and cell cycle exit in quiescent cells.**

Monitoring Editor
Carl-Henrik Heldin
Ludwig Institute for Cancer Research

Received: Jul 18, 2012
Revised: Jul 8, 2013
Accepted: Jul 29, 2013

INTRODUCTION

Proper formation of tissues and organisms requires that cells have the capacity to transition between a proliferative, cycling state and a resting state outside the proliferative cell cycle termed quiescence. Cells integrate cues from growth factors, other cells, and extracellular matrix proteins and interpret these signals as they decide whether to commit to proliferation or quiescence. The ability of cells to properly exit the cell cycle, retain viability during quiescence, and return to the cell cycle when needed is necessary for complex multicellular processes such as growth and healing. Cells that fail to quiesce properly can contribute to the formation of tumors.

The transition between an out-of-cycle, quiescent state and a proliferative state is associated with changes in gene expression patterns (Schneider *et al.*, 1988; Coppock *et al.*, 1993; Venezia *et al.*, 2004; Coller *et al.*, 2006) and, in some systems, changes in overall transcription rates (Jaehning *et al.*, 1975). These changes in gene expression with quiescence may be accompanied and regulated by alterations in the packing of DNA as chromatin (Tokuyasu *et al.*, 1968; Dardick *et al.*, 1983; Setterfield *et al.*, 1983). In particular, modifications of lysines on the tails of histones H3 and H4 play an important role in local control of transcriptional activation and silencing, and the information encoded in these tails may constitute a code interpreted by proteins that bind to specific modifications (Jenuwein and Allis, 2001).

This article was published online ahead of print in MBoC in Press (http://www.molbiolcell.org/cgi/doi/10.1091/mbc.E12-07-0529) on August 7, 2013.

The authors declare that they have no conflict of interest.

H.C., B.G., and A.E. designed experiments. A.M. performed the FISH experiments reported in Figures 1 and 7. A.E. and X.W. performed the experiments reported in Figure 5. A.E. performed the remaining experiments. H.C. and A.E. wrote the manuscript, and all other authors contributed comments.

Address correspondence to: Hilary A. Coller (hcoller@ucla.edu).

Abbreviations used: 14dCI, 14 d of contact inhibition; P, proliferating.

When proliferating cells enter S phase, their histones are incorporated into chromatin unmodified. Most lysines are quickly modified, however, likely using the existing chromatin as a template to transfer information. One lysine in particular does not become modified immediately after deposition—lysine 20 on H4 (Pesavento *et al.*, 2008; Zee *et al.*, 2012). H4K20 becomes monomethylated only during M phase as a result of mechanisms that limit the expression and activity of PR-Set7, the methyltransferase (Fang *et al.*, 2002; Nishioka *et al.*, 2002). PR-Set7 is actively targeted for proteasome-mediated degradation in S phase (Julien and Herr, 2004; Abbas *et al.*, 2010; Wu *et al.*, 2010; Jorgensen *et al.*, 2011). The M-phase specific phosphorylation of PR-Set7 at serine 29 occurs at the onset of mitosis and contributes to stabilization of the enzyme (Wu *et al.*, 2010). In addition, PHF8, an H4K20me1 demethylase, is removed from chromatin in prophase, allowing for an accumulation of H4K20me1 (Liu *et al.*, 2010). Dimethylated and trimethylated H4K20 do not fluctuate as widely as the monomethyl form during the cell cycle. H4K20me2 is the most abundant form in *Drosophila* (Yang *et al.*, 2008) and human cells (Young *et al.*, 2009), existing on ~80% of histones. Trimethylated H4K20 is the least abundant of the three forms and is associated with repeated sequences (Kourmouli *et al.*, 2004; Martens *et al.*, 2005; Phalke *et al.*, 2009). Knockouts of the enzymes that modify H4K20 display a variety of phenotypes. PR-Set7–knockout mice lose all H4K20 modifications and are embryonic lethal. A conditional knockout in embryonic stem cells leads to chromatin condensation defects (Oda *et al.*, 2009). Knockout of both Suv4-20h1 (the enzyme that converts the monomethylated form to the dimethylated form) and Suv4-20h2 (the enzyme that converts the dimethylated form to the trimethylated form) leads to loss of the H4K20me2 and H4K20me3 histone forms and is perinatally lethal (Schotta *et al.*, 2008). Loss of these modifications in mouse cells leads to telomere elongation (Benetti *et al.*, 2007; Marion *et al.*, 2011).

Studies examining the distribution of bulk levels of histone modifications in quiescent and proliferating lymphocytes have revealed differences in the levels of specific histone modifications between the two states. In response to antigen, lymphocytes can be stimulated from their quiescent state to divide. This reactivation is associated with an unpacking of the tightly wound heterochromatin and physical relocalization of specific histone modifications within the nucleus (Tokuyasu *et al.*, 1968; Dardick *et al.*, 1983; Setterfield *et al.*, 1983; Grigoryev *et al.*, 2004). Activation of B cells is associated with increased levels of multiple histone modifications (Baxter *et al.*, 2004). Lymphocyte activation is also associated with changes in the intranuclear localization of specific histone modifications. H4K12Ac, for instance, was excluded from centromeric heterochromatin in quiescent lymphoyctes and was redistributed more uniformly upon activation (Grigoryev *et al.*, 2004).

Primary dermal fibroblasts represent another cell type that can transition between a quiescent and a proliferative state. Fibroblasts are often quiescent in vivo. Their physiological role is to secrete extracellular matrix proteins that give tissue its strength and resilience. Fibroblasts can also proliferate, for instance, to replenish dead cells, and upon activation in the context of a wound. Early studies indicated a likely transition in chromatin structure upon stimulation of quiescent fibroblasts based on circular dichroism (Chiu and Baserga, 1975). We therefore set out to address whether fibroblasts undergo changes in chromatin compaction and histone modifications upon quiescence. We used fluorescence in situ hybridization (FISH) for two loci on opposite arms of a single chromosome to quantitatively assess chromatin compaction. We also used a mass spectrometry–based method (Plazas-Mayorca *et al.*, 2009) to measure the levels of ~50 histone modifications. With these approaches, we characterized changes in chromatin compaction and histone modifications as fibroblasts transition from proliferation to contact inhibition–induced quiescence. We further defined changes in histone modifications with time during quiescence, over the course of the cell cycle, and in cells that are terminally arrested and have entered senescence. Our findings highlight the importance of methylation on H4K20. The singly methylated form of H4K20 is enriched in mitotic cells, whereas in quiescent cells, the levels of H4K20me2 and H4K20me3 increase. This specific lysine, in its different forms, plays a role in mitosis and during quiescence, facilitating compaction and the transition between proliferative and quiescent cell cycle states.

RESULTS

Contact inhibition in fibroblasts is associated with chromatin compaction

We established a model system of quiescence in which primary human dermal fibroblasts are sampled either proliferating or after being induced into quiescence by contact inhibition (Lemons *et al.*, 2010). We sought to determine whether the quiescent state achieved when primary human fibroblasts are contact inhibited is associated with a change in chromatin compaction. We collected proliferating (P), 14 d contact–inhibited (14dCI), and restimulated fibroblasts (Figure 1, A–C) and used dual-color FISH with probes for two loci on chromosome 16 to monitor the extent of chromatin compaction. This technique has been used as a global measure for chromatin compaction (Bystricky *et al.*, 2004; Chambeyron and Bickmore, 2004; Centore *et al.*, 2010). The distance between the two probes was measured in ~50 cells in each state, and the average distance was calculated. In quiescent, contact-inhibited fibroblasts, the average distance between these loci was shorter than in proliferating fibroblasts (Figure 1, D and E). Fibroblasts that were restimulated to enter the cell cycle contained the largest average interlocus distance. Thus, entry into quiescence in response to contact inhibition results in more tightly packed chromatin that is reversibly unpacked upon stimulation.

H4K20 is differentially methylated in quiescent fibroblasts

Given our observation that contact-inhibited fibroblasts pack chromatin more tightly than proliferating or restimulated fibroblasts, we sought to uncover histone modification changes that are associated with quiescence in this system. To quantitatively measure the global changes in steady-state levels of histone modifications between P and 14dCI fibroblasts, we analyzed histones by liquid chromatography-mass spectrometry (LC-MS/MS). Mass spectrometry allows for a highly quantitative analysis of ~50 histone modifications in a single experiment, eliminating the need to select specific modifications for analysis before performing the experiment. Histones were extracted from primary human fibroblasts using acid extraction (Shechter *et al.*, 2007) and modified with propionic anhydride to block unmodified and monomethylated lysines. Histones were digested with trypsin (cleaving only at arginine residues) and analyzed by LC-MS/MS. The intensity values for all modification states of a given peptide were used to calculate the fraction of the peptide in each individual modification state. Differential labeling of peptide N-termini with hydrogen-containing or deuterium-containing propionic anhydride was used to analyze two samples simultaneously and calculate fold changes between conditions, similar to microarray analysis.

Surprisingly, after 14 d of contact inhibition, despite the fact that the proliferating but not quiescent cells must replace their histone modifications with each cell division, the majority of histone

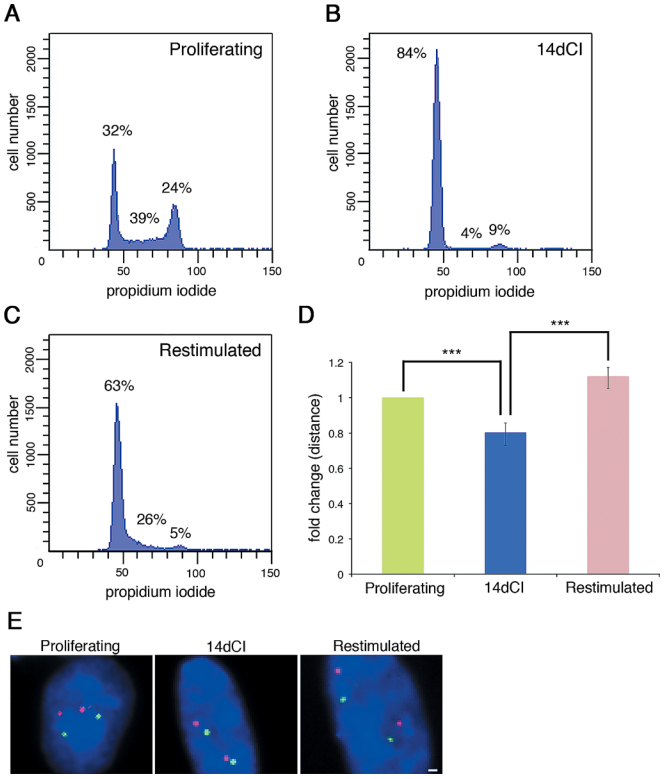

FIGURE 1: Contact-inhibited fibroblasts exhibit increased chromatin compaction. (A–C) Proliferating, contact-inhibited (14 d), and restimulated fibroblasts were collected and analyzed by propidium iodide staining and flow cytometry. FlowJo analysis was performed to estimate the fraction of cells in G1, S, and G2/M phases. (D) Cells were fixed, and dual-colored FISH probes were used to visualize 16q22 and 16p13. Approximately 30–100 cells were measured, and the average distance between the foci was determined. Mean and SE are plotted. Contact-inhibited fibroblasts exhibited a smaller interprobe distance than proliferating ($p = 7.5 \times 10^{-4}$) and restimulated ($p = 6.4 \times 10^{-8}$) cells. (E) Representative images of FISH on both copies of chromosome 16 for P, 14dCI, and restimulated fibroblasts. Each arm of chromosome 16 is marked with a different color to visualize the distance between the arms. Scale bar, 2 μm.

modifications were present at similar levels in proliferating and quiescent fibroblasts (Figure 2A). Of the 48 modification states monitored, there were 44 with less than a twofold change. This suggests that when fibroblasts transition between proliferation and quiescence, they mostly maintain similar steady-state histone modification levels. The results do not rule out a difference in the rates at which these modifications are added and removed, and we explore this question elsewhere (Evertts *et al.*, 2013). It also does not rule out changes in the locations of the modifications, which can be addressed using chromatin immunoprecipitation (ChIP) sequencing.

Some lysines did show differential levels of histone modifications between P and 14dCI (Figure 2, C and D). On histone H3, K9 and K27 were more likely to be methylated in quiescent fibroblasts than proliferating fibroblasts. Lysine 9 methylation was increased in quiescent cells, as indicated by a loss of unmodified H3K9. For H3K27, the most prominent change was that quiescent fibroblasts contained higher levels of H3K27me2 and H3K27me3, especially in combination with modified K36. The largest changes between P and 14dCI histones occurred on H4K20 (Figure 2, C and D, and Supplemental Figure S1). H4K20 can exist in four distinct forms with no methylation or one, two, or three methyl groups, each of which has been reported to play a different cellular role. In quiescent fibroblasts, the fraction of H4K20 that is unmodified or contains a single methyl group decreased >2-fold, whereas the fraction of H4K20 that is modified with two or three methyl groups increased 2- and 10-fold, respectively. We used an antibody specific for the trimethyl form to confirm and validate the increase in H4K20me3 during quiescence and also found that the modification level is reversed after 48 h of restimulation (Figure 2B and Supplemental Figure S2). Immunofluorescence with the same antibody indicated that H4K20me3 was higher in abundance in the nucleus of quiescent versus proliferating fibroblasts, although a recognizable difference in the distribution pattern was not observed between the two states (Supplemental Figure S3). Thus, although most histone modifications are found at similar steady-state levels in proliferating and contact-inhibited fibroblasts, there were some histone lysines with reproducibly different levels of methylation.

G_1-enriched fibroblasts show differential H4K20 methylation patterns compared with quiescent fibroblasts

The asynchronous proliferating cells that we monitored were a mixture of cells in all phases of the cell cycle, whereas quiescent cells were mostly in the G_0/G_1 cell cycle phase (Figure 1). To determine whether there are histone modifications associated specifically with quiescence or G_0, we compared histone modifications in quiescent cells with histone modifications in a purified population of G_1 cells, based on the expectation that quiescent cells exit the cell cycle from G_1 (Pardee, 1974). In this way, we eliminated the effects of changes in histone modifications over the cell cycle. Fibroblasts were synchronized with serum starvation and hydroxyurea treatment. Cells were released from a G_1/S block via hydroxyurea and collected 12 h later in early G_1. The G_1-enriched fibroblasts were compared with 14dCI fibroblasts using LC-MS/MS (Figure 2A). Most lysines had similar levels of modifications in G_1-enriched fibroblasts compared with 14dCI fibroblasts, which is in accord with the finding that P and 14dCI cells had similar levels of most histone modifications. The increase in methylation on K27 observed in P versus 14dCI cells was reduced with G_1-enriched fibroblasts, suggesting that K27 methylation fluctuates moderately over the cell cycle. We address this further later. For H4K20, however, 14dCI fibroblasts contained higher levels of dimethylated and trimethylated forms when compared not only to proliferating cells but also to G_1-enriched cells. Thus these changes are associated with quiescence and do not reflect a stalling in G_1.

We identified six modifications that changed significantly in 14dCI versus G_1-enriched fibroblasts, including H4K20me2 and H4K20me3 (Figure 2, C and D). All six modifications also change significantly between 14dCI and P cells. Unmodified H3K9/K14 and unmodified H3K27/K36 were statistically significant but very modestly repressed in quiescent compared with G_1 cells. H3K36me1 and H3K27me3K36me1 were statistically significantly but very modestly increased in quiescent compared with G_1 cells. In contrast, large changes were observed for H4K20. 14dCI fibroblasts contained a twofold increase in the fraction of lysines in the dimethylated form. Because many histones in the cell are in the H4K20me2 form, this twofold change translates to ~34% increase in the amount of histones present in the dimethylated form in 14dCI cells (Figure 2D). H4K20me3 is a rare modification representing only 0.2% of H4K20 in proliferating fibroblasts. Its levels were increased approximately eightfold in 14dCI fibroblasts, in which it represented ~1.4% of all H4K20.

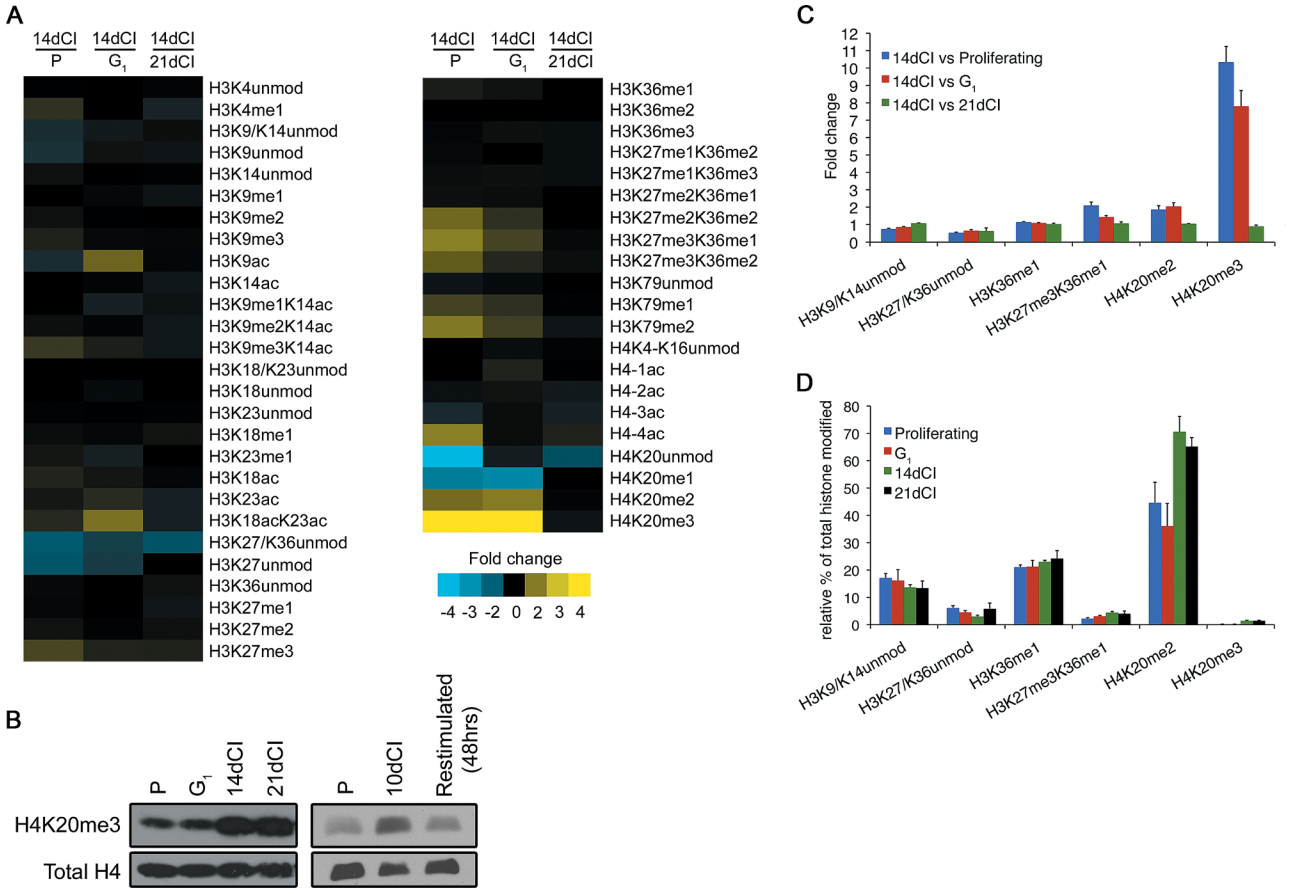

FIGURE 2: Modification status of H4K20 changes as fibroblasts become quiescent. The relative abundances of detectable histone modifications on histones H3 and H4 were determined for P, G_1-enriched, 14dCI, and 21dCI fibroblasts using (LC-MS/MS). P, G_1-enriched, and 21dCI histones were compared with 14dCI histones by labeling the N-termini of histones with hydrogen- or deuterium-containing propionic anhydride. The values for all modification states on each peptide were used to determine relative abundance for each individual modification state for both samples analyzed together. (A) The $\log_2$ fold changes of 14dCI vs. proliferating, G_1-enriched, and 21dCI are shown in heat map format. Data represent averages from three independent experiments. (B) Western blotting shows a similar change in abundance of H4K20me3 in noncycling states and cycling states. A pan-H4 antibody was used as a loading control. (C) Six modifications exhibited statistically significant differences (*t* test, $p < 0.05$) between G_1-enriched and 14dCI fibroblasts. The data from A are plotted to show the fold change between 14dCI and proliferating, G_1-enriched, and 21dCI fibroblasts. Error bars indicate SE. (D) Percentage of total histones modified for each of the six significant modifications.

Histone modification patterns are maintained during contact inhibition

We then tested whether the changes in histone modifications observed at 14 d of contact inhibition would be maintained if the cells remained contact inhibited for a longer period of time. We compared the pattern of histone modifications in 14dCI fibroblasts with the pattern in 21dCI fibroblasts (Figure 2A). An additional 7 d of contact inhibition did not further increase or decrease histone modification levels, including on H4K20, suggesting that the changes in histone modification levels achieved by 14 d of contact inhibition were preserved when cells were maintained in a contact-inhibited state for a longer period of time.

H4K20me1 levels increase over the course of the cell cycle and are converted to H4K20me2 and H4K20me3 in quiescence

Our discovery that there were differences in histone modifications between a G_1-enriched cell population and an asynchronous proliferating population suggested that there are changes in histone modifications during cell cycle progression (Pesavento *et al.*, 2008; Schulze *et al.*, 2009). To address this question, we monitored histone modifications over the cell cycle in primary fibroblasts using LC-MS/MS (Figure 3A). Cells were synchronized with serum starvation and hydroxyurea treatment and collected in S, G_2/M, and G_1 phases (Figure 3, B–E). Histones were extracted and analyzed together with 14dCI histones to generate a fold-change difference between 14dCI and each cell cycle phase. The fold change was normalized across each modification so that decreases represent lower amounts of the modification relative to the average of all phases, and increases represent higher amounts of the modification relative to the average of all phases. The majority of modifications do not change as the cells pass through S phase and into other phases (Figure 3A). This suggests that most lysines are rapidly modified at the replication fork or soon after and that the cell maintains comparable levels of most modifications throughout the cell cycle. For instance, the different modified forms of two lysines that have been studied extensively in the literature for their roles in transcription, H3K9 and H3K27, are present at relatively stable levels across cell cycle phases, with some slight variations that are most pronounced in the dimethylated forms (Figure 4, A and B).

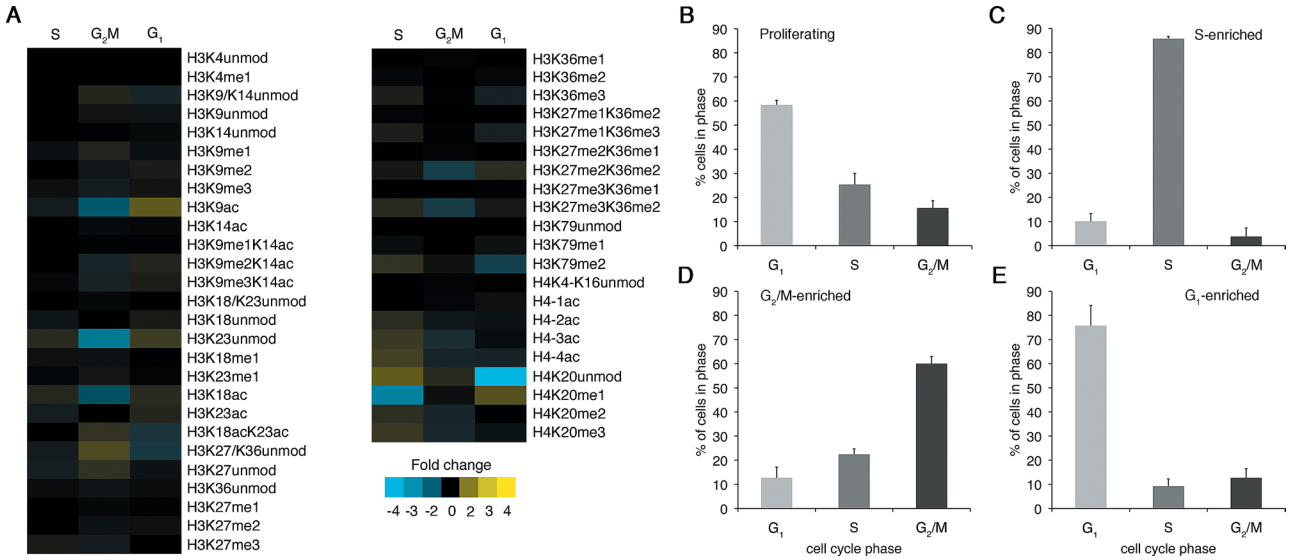

FIGURE 3: Cell cycle–dependent changes in histone modification levels. The relative abundances of histone modifications were determined for S phase–enriched, G_2/M-enriched, and G_1-enriched fibroblasts using LC-MS/MS. (A) The $\log_2$ fold change for each phase relative to the average of all phases for each modification in heat map format. Data represent means from three independent experiments for S and G_1 and two independent experiments for G_2/M. (B–E) Propidium iodide staining and flow cytometry were used to generate cell cycle profiles for (B) asynchronously proliferating fibroblasts and cells enriched in (C) S phase, (D) G_2/M phase, and (E) G_1 phase. Data represent the mean of three independent experiments. Error bars indicate SE.

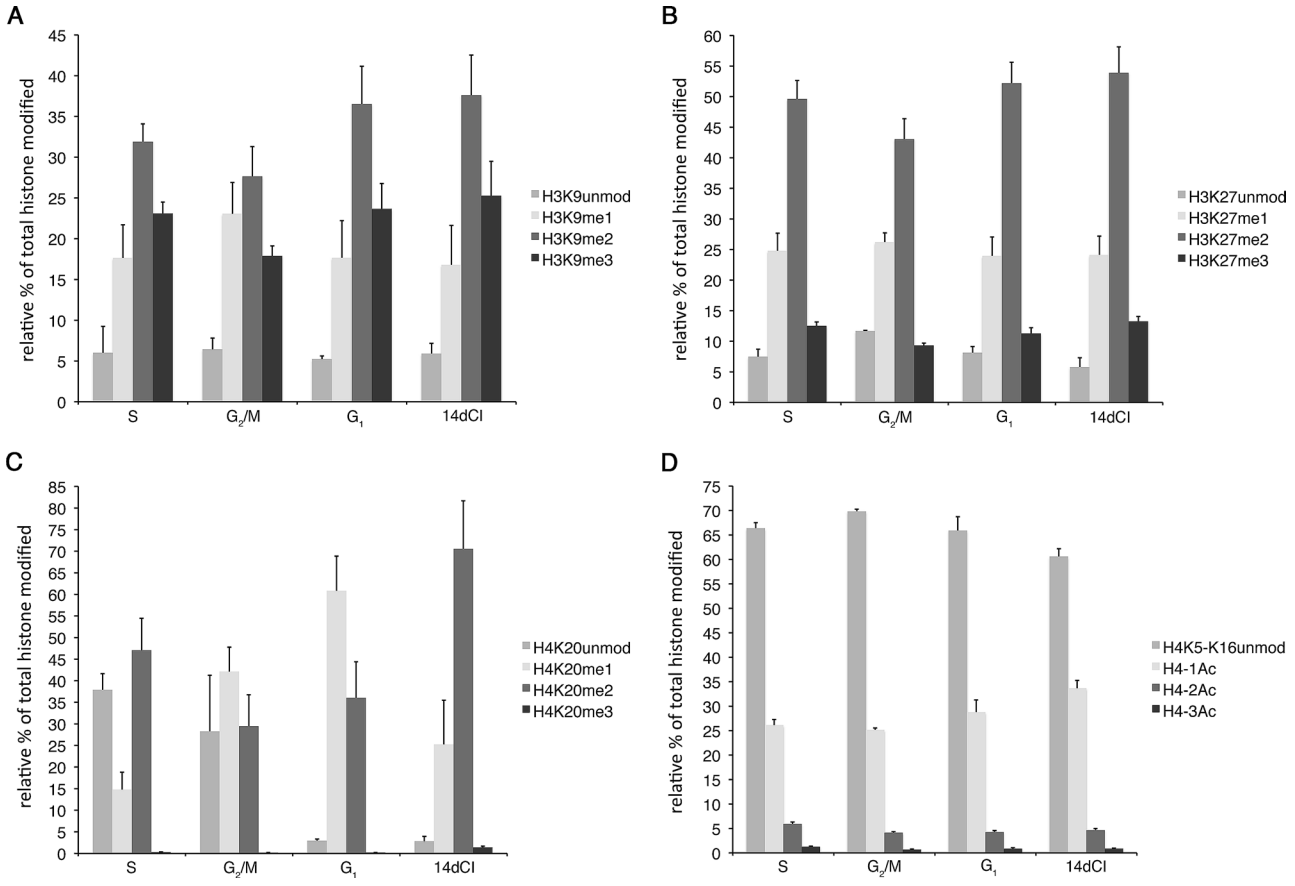

FIGURE 4: Modification states of H4K20 exhibit the greatest fluctuation across the cell cycle among histone lysines. The relative percentage of modified histones was calculated using mass spectrometry data for histone modifications in S, G_2/M, G_1, and 14dCI. The relative distribution of methylated forms is plotted for (A) H3K9, (B) H3K27, (C) H4K20, and (D) acetylated H4 on lysines 5–16. Error bars indicate SE.

One lysine, H4K20—the same lysine that exhibited the largest changes between proliferating and quiescent fibroblasts—did display large changes in modification levels across the cell cycle (Figure 4C). This is consistent with reports that H4K20 methylation status is cell cycle dependent (Jorgensen *et al.*, 2007; Pesavento *et al.*, 2008; Oda *et al.*, 2009; Abbas *et al.*, 2010; Centore *et al.*, 2010; Wu *et al.*, 2010). The unmodified form of histone H4K20 was present at its highest level among the cell cycle states during S phase. It decreased as the cells moved into G_2/M and G_1 and remained low in quiescent cells. Levels of H4K20me1 were low in S phase and progressively increased in G_2/M. H4K20me1 levels were lower in 14dCI than in G_1 cells, although the result is not statistically significant. Levels of H4K20me2 were relatively stable throughout the cell cycle but increased in quiescence. Levels of H4K20me3 were also relatively constant and very low over the course of the cell cycle but rose in quiescent fibroblasts. Other lysines on H4, such as H4K5-K16, did not exhibit the same pattern of increased modification over the course of the cell cycle as H4K20 (Figure 4D). The results indicate that H4K20, in its unmodified and monomethylated states, is the lysine that exhibits the greatest changes over the course of the cell cycle and exhibits the largest changes with quiescence.

Modification levels in senescence are similar to those in quiescence

Quiescent fibroblasts have the ability to reenter the cell cycle and proliferate after a period of cell cycle arrest. Other cells, such as senescent or terminally differentiated cells, remain in a state of cell cycle arrest and do not routinely reexpress proliferation-associated genes. We sought to compare histone modifications in reversibly arrested cells with those of permanently arrested cells by extending our analysis to senescent fibroblasts. A retroviral vector expressing an oncogenic form of the Ras protein (G12V) was introduced into fibroblasts. Ras^{G12V}-overexpressing fibroblasts grew rapidly and then ceased division and became senescent. Immunoblotting confirmed higher Ras levels in engineered fibroblasts compared with cells transduced with a control vector (Figure 5A). β-Galactosidase staining confirmed that the Ras^{G12V}-overexpressing cells had entered senescence (Figure 5B). LC-MS/MS analysis of histones in senescent fibroblasts indicated that the levels of H4K20 modifications are similar between quiescence and senescence (Figure 5C). This suggests that changes in the pattern of H4K20 methylation occur during other types of cell cycle arrest and not just during quiescence.

Overexpression of Suv4-20h1 causes an increase in the fraction of cells in G_2

Most H4K20 lysines are in a dimethylated form in fibroblasts that were contact inhibited for 14 d. To assess whether a shift from the monomethylated to dimethylated form of H4K20 contributes to cell cycle exit, we overexpressed the enzyme that catalyzes the transition from H4K20me1 to H4K20me2 (Suv4-20h1) in fibroblasts (Figure 6). Fibroblasts were transduced with a retrovirus containing Suv4-20h1 driven by a cytomegalovirus promoter and allowed to recover for 24 h after selection with puromycin. Fibroblasts overexpressing Suv4-20h1 were larger and more flattened than control cells (Figure 6, B and D). The cell cycle profile of control and Suv4-20h1–overexpressing fibroblasts was determined by staining cells with propidium iodide, followed by flow cytometry analysis. Overexpression of Suv4-20h1 caused a decrease in the fraction of cells in S phase and an increase in the fraction of cells in G_2/M ($p = 0.02$, paired *t* test; Figure 6, A, C, and E), whereas overexpression of

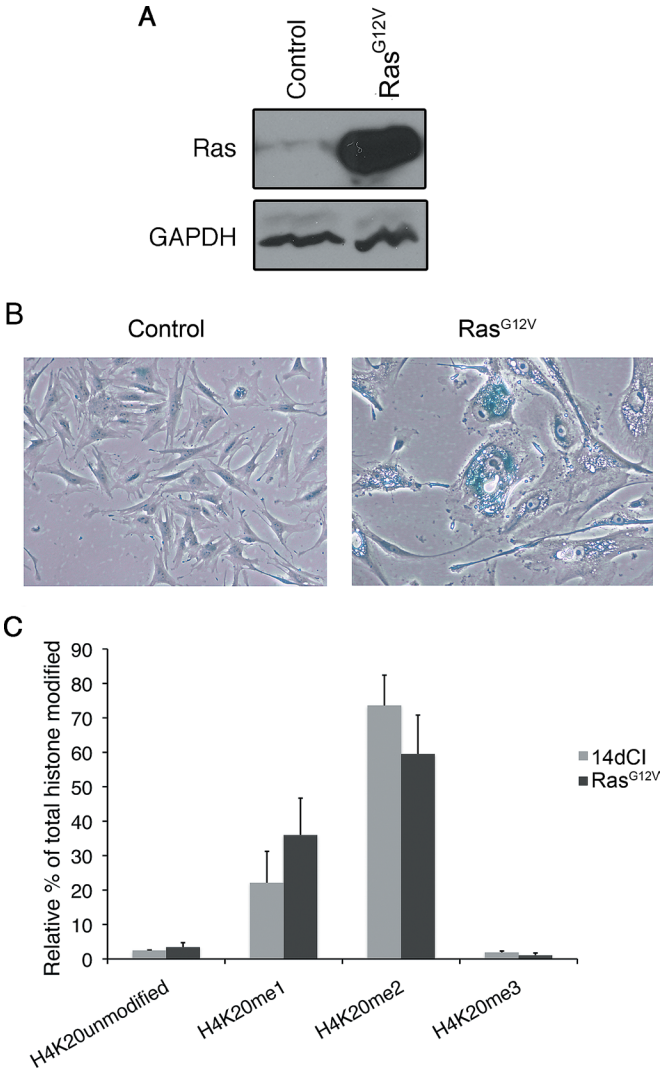

FIGURE 5: Histone analysis of senescent fibroblasts. Fibroblasts were transduced with a retrovirus containing an empty pBABE vector or pBABE-Ras^{G12V}. (A) Immunoblotting was performed to detect the expression of Ras. (B) β-Galactosidase expression was detected in cells transduced with a control vector and cells expressing Ras^{G12V} by fixing cells and incubating with X-gal. (C) Mass spectrometry was performed on control cells that were 14dCI and Ras^{G12V}-expressing cells that were senescent. Relative percentage of modifications on H4K20 are plotted. Error bars indicate SE.

Suv4-20h2 did not alter the cell cycle profile significantly (Figure 6F). Suv4-20h1–overexpressing cells were also stained with a histone 3 phospho-S10 antibody, an M-phase marker. Fewer phosho-S10–positive cells were observed in Suv4-20h1–overexpressing cells, indicating G2 arrest (Supplemental Figure S5). Finally, the same cells were stained with X-gal to measure the level of senescence-associated β-galactosidase expression and were determined to have higher levels of senescence than control cells (Supplemental Figure S6). Thus a shift in the fraction of histone H4K20 containing the dimethylated rather than monomethylated form had a significant effect on cell cycle progression.

Knockdown of Suv4-20h1 and Suv4-20h2 results in loss of compaction

To further explore the possible importance of the trimethylated form of H4K20, the form that displays the largest increase in quiescent

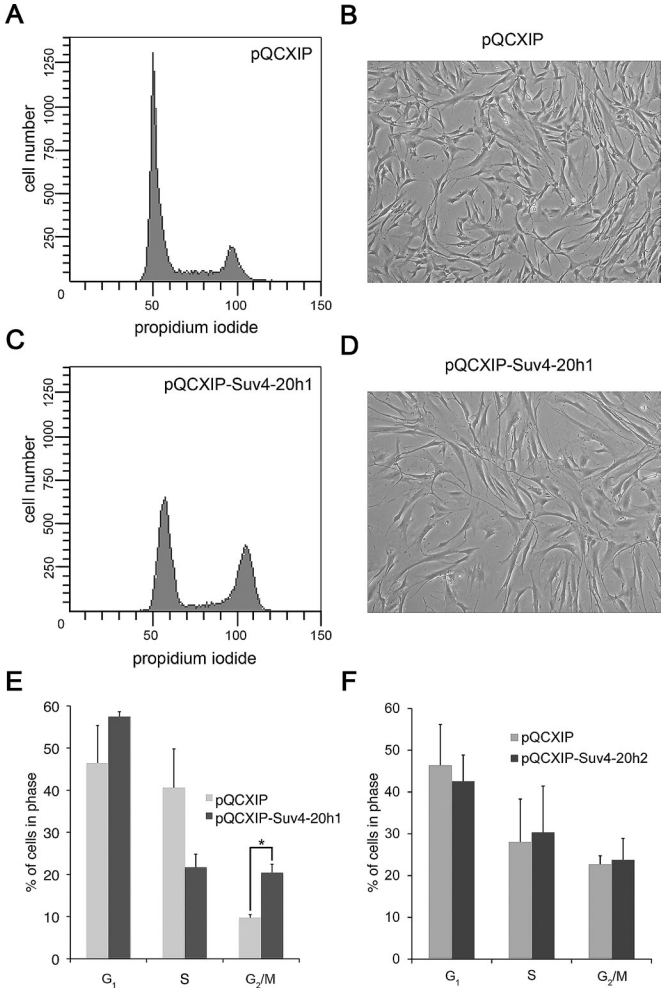

FIGURE 6: Overexpression of Suv4-20h1 induces G_2/M arrest. (A–D) Fibroblasts were transduced with a retrovirus containing an empty expression vector or vectors expressing Suv4-20h1 or Suv4-20h2. (A, C) Control and Suv4-20h1–expressing cells were stained with propidium iodide and analyzed by flow cytometry. (B, D) Light microscopy images (4×) were taken to show overall cell morphology. The experiment was performed three times; representative data are shown. (E, F) Percentages of cells in G_1, S, and G_2/M were determined using FlowJo software and plotted for control and Suv4-20h1– and Suv4-20h2–expressing cells. Error bars indicate SE.

cells, we also generated fibroblasts with retroviral vectors containing knockdown of both Suv4-20h1 and Suv4-20h2. Mass spectrometry was used to monitor the reduction of both modifications. H4K20me2 was reduced by ~30%, and H4K20me3 was reduced by ~70% (Figure 7A). We analyzed intrachromosome distances using dual-color FISH, as described earlier, in shControl and shSuv4-20h1/h2 cells and discovered that this distance increased 1.2-fold in the knockdown cells, $p = 1.2 \times 10^{-6}$ (analysis of variance [ANOVA]; Figure 7B). Representative images show the decreased compaction observed in shSuv4-20h1/h2 cells (Figure 7C). A more extreme example of the decreased compaction is shown in Figure 7C, right, and was observed only in shSuv4-20h1/h2 cells. We also monitored the amount of compaction in cells with individual knockdowns of Suv4-20h1 and Suv4-20h2 using small interfering RNAs (siRNAs). We found that a reduction of either methyltransferase caused an ~15% increase in the distance between FISH probes, which is similar to the effect observed with the shSuv4-20h1/h2 double knockdown. The Suv4-20h1 siRNA increased the distance between FISH probes but did not achieve statistical significance, whereas treatment with the Suv4-20h2 siRNA did produce a statistically significant change in compaction ($p = 0.01$; paired t test). These results are consistent with previous reports that the trimethyl form of H4K20 promotes compaction (Lu *et al.*, 2008), as intrachromosomal locus distances increased in cells with lower levels of this modification.

Knockdown of Suv4-20h1 and Suv4-20h2 results in increased S-phase cells and defects in quiescence entry

To determine the effect of the loss of H4K20me2 and H4K20me3 on proliferation and quiescence, we transfected cells with a pool of four siRNAs targeting Suv4-20h1 and Suv4-20h2 (four sequences for each transcript). Cells were transfected twice, which resulted in a reduction in the levels of the targeted transcripts (Supplemental Figure S7). At 24 h after the second transfection, cells were treated with the modified nucleotide 5-ethynyl-2′-deoxyuridine (EdU) for 2 h. The incorporated EdU was detected using a chemically bound fluorophore and analyzed by flow cytometry (Click-iT EdU). The percentage of cells that were in S phase or entered S phase in the 2-h labeling was significantly higher for fibroblasts transfected with siSuv4-20h1/h2 than for a control set of siRNAs (Figure 8A). We next assessed whether knockdown of Suv4-20h1/h2 affects the ability of fibroblasts to exit the proliferative cell cycle in response to quiescence cues. We serum starved fibroblasts and monitored the fraction in S phase 24 h later with Click-iT EdU. We discovered that cell populations in which Suv4-20h1/h2 was depleted contained a greater fraction of cells in S phase than controls (Figure 8A). By performing the experiment with pools of siRNAs specific for either Suv4-20h1 or Suv4-20h2, we discovered that Suv4-20h2 was the enzyme responsible for the S-phase phenotype (Figure 8A), as a reduction in Suv4-20h1 showed similar levels of S-phase cells, and knockdown of Suv4-20h2 resulted in more S-phase cells. We then tested whether Suv4-20h2 knockdown alone could lead to resistance to contact inhibition and found that after 48 h of contact inhibition, the population of cells transfected with the siSuv4-20h2 contained more cells in S phase (Figure 8A). To eliminate the possibility of off-target effects from the siRNA pools, we performed knockdown experiments with individual siRNAs for both the control and Suv4-20h2 (Figure 8B). Transfection with three of the four Suv4-20h2 sequences resulted in more S-phase cells compared with the control sequences, suggesting that the results are not a consequence of off-target effects of the siRNAs. These findings indicate that not only do the levels of the higher methylated forms of H4K20 increase with quiescence, but the methylation state of H4K20 plays a functional role in the control of cell cycle progression, with the trimethyl H4K20 maintaining cells in a noncycling state (Figure 9).

DISCUSSION

Previous studies in lymphocytes (Baxter *et al.*, 2004; Grigoryev *et al.*, 2004) and mesodermal precursors (Schubeler *et al.*, 2000; Zhang *et al.*, 2002; Caretti *et al.*, 2004; Mal, 2006) revealed that quiescence in these cell types is associated with large changes in the levels of many histone modifications. Our data, in contrast, demonstrate that proliferating and contact-inhibited fibroblasts contain similar steady-state, global levels of most histone modifications. Our data are in accord with a recent study in which quiescence in T-lymphocytes was not associated with changes in the global levels of histone modifications but instead with chromatin condensation by the condensin II complex (Rawlings *et al.*, 2011). Our results indicating similar levels of histone modifications in proliferating and quiescent fibroblasts for most modifications are also consistent with our previous data

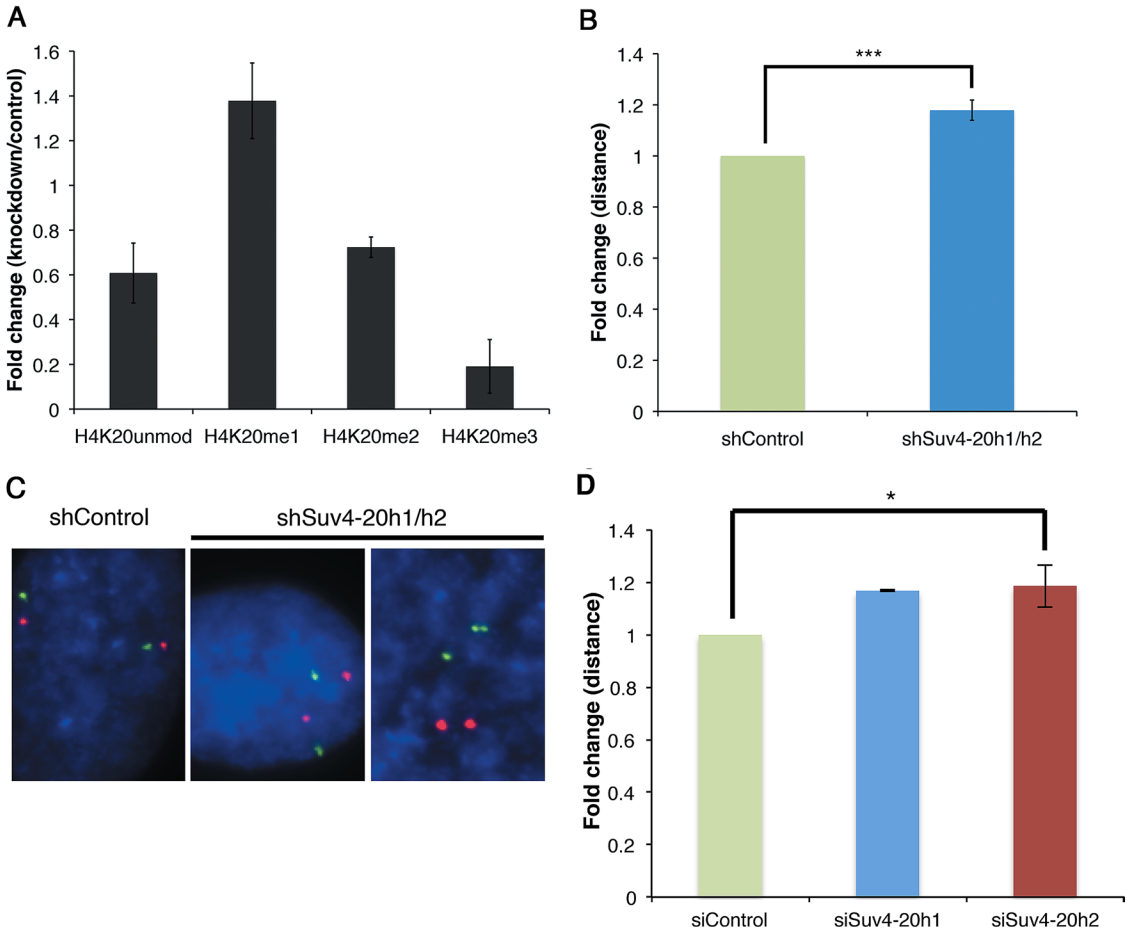

FIGURE 7: Suv4-20h1 and Suv4-20h2 knockdown results in decreased compaction. shRNAs were stably integrated and expressed in fibroblasts. Nonspecific sequences were expressed in the control cells, and sequences targeting Suv4-20h1 and Suv4-20h2 were used to reduce H4K20me2 and H4K20me3. (A) Histones were analyzed by mass spectrometry, and the fold change was plotted for shSuv4-20h1/h2 cells vs. shControl. (B) Dual-colored FISH was used to measure the distance between both arms of chromosome 16 in shControl and shSuv4-20h1/h2 cells ($p = 1.2 \times 10^{-6}$; ANOVA). (C) Representative images from FISH experiments depicting both copies of chromosome 16 with each arm identified with a different color. Right, shSuv4-20h1/h2, an example of more extreme decompaction. (D) siRNA sequences were used to reduce the expression of Suv4-20h1 or Suv4-20h2 individually. FISH was used to measure chromosome 16 compaction in siControl, siSuv4-20h1 ($p = 0.055$; paired t test), and siSuv4-20h2 cells ($p = 0.01$; paired t test).

indicating that contact-inhibited fibroblasts both repress and activate genes upon entering quiescence (Coller *et al.*, 2006; Pollina *et al.*, 2008; Lemons *et al.*, 2010) and maintain high metabolic rates (Lemons *et al.*, 2010). Although global levels do not change for most modifications, however, the positions of the modifications within chromatin could shift dramatically between proliferating and quiescent fibroblasts. ChIP-sequencing experiments using antibodies that bind these histone modifications would address whether quiescence is associated with a redistribution of activating or repressive marks among promoters to accommodate a new transcriptional program.

Histone modifications have been shown to vary across the cell cycle. One report shows that H3K79me2 levels peak in *Saccharomyces cerevisiae* at G_2/M and the enzyme responsible for creating the mark (Dot1) is dependent on SBF, a cell cycle–regulated protein complex (Schulze *et al.*, 2009). Knockdown of Dot1L in small-cell lung cancer cells resulted in a proliferation block and display of senescence characteristics, further linking this modification to the cell cycle (Kim *et al.*, 2012). We did not measure a large change in either H4K79me2 or H4K79me3 with our methods in human fibroblasts.

In contrast, the methylation status of H4K20, a lysine that is not conserved in *S. cerevisiae*, varied dramatically over the course of the cell cycle in the human fibroblasts we studied. Previous reports based on mass spectrometry analysis in HeLa cells showed that new H4K20 is unmodified in S phase and becomes monomethylated only in M phase (Pesavento *et al.*, 2008; Zee *et al.*, 2012) via specific regulation of PR-Set7. We also show an increase of H4K20me1 during G_2/M and early G_1 relative to S phase. H4K20 then shifts from being highly enriched with monomethyl to predominantly dimethyl and trimethyl when cells become quiescent. Although H4K20me1 has a critical function in M phase, quiescent cells contain lower levels of the monomethylated form and higher levels of dimethylated and trimethylated forms.

The H4K20 methylation profile is distinct in quiescent fibroblasts from its profile at any point in the cell cycle. In quiescent fibroblasts, the dimethylated and especially trimethylated forms accumulate (Sarg *et al.*, 2002; Kourmouli *et al.*, 2004). This methylation pattern

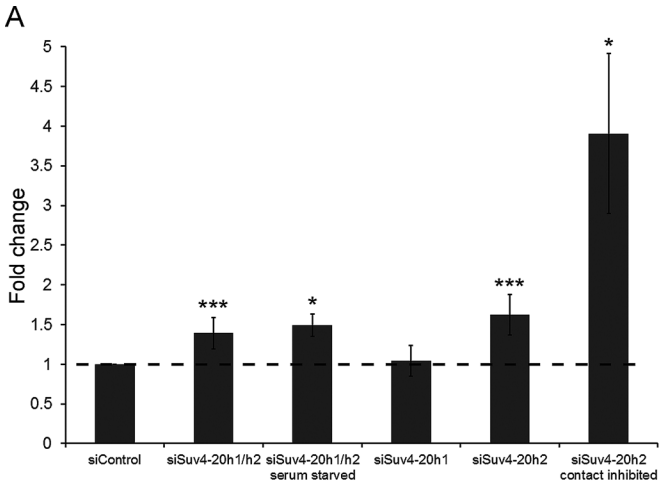

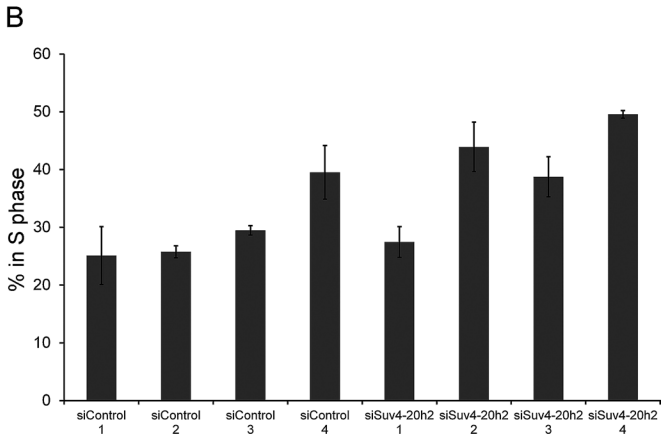

FIGURE 8: Knockdown of Suv4-20h2 results in a higher fraction of cells in S phase in full serum and after induction into quiescence. Fibroblasts were treated with the nucleotide analogue EdU for 2 h, stained with DAPI, and analyzed by flow cytometry to determine the fraction of cells in S phase. (A) A pool of 4 siRNAs was used to reduce the expression of Suv4-20h1 and Suv4-20h2. A nontargeting pool was used as a control. Cells were analyzed in full serum and after 24 h of serum starvation. Cells were also analyzed after transfection with either a pool of siRNAs targeted against Suv4-20h1 or a pool of siRNAs targeted against Suv4-20h2. Contact-inhibited cells were analyzed with Suv4-20h2 siRNAs only. (B) Cells with full serum were treated with one of four individual control siRNAs or one of four siRNAs targeting Suv4-20h2, and the fraction of EdU-positive cells was measured.

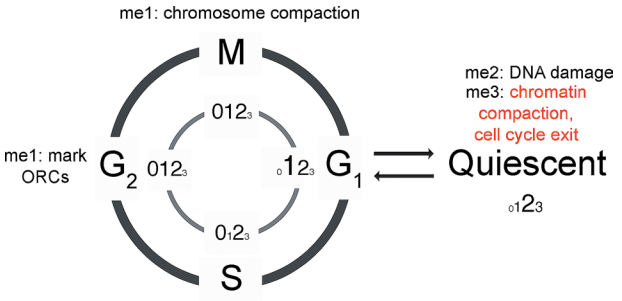

FIGURE 9: Model for H4K20 methylation with cell cycle exit. The relative levels of H4K20 methylation are shown for the four possible modification states: unmodified (0), monomethyl (1), dimethyl (2), and trimethyl (3). Modification levels are shown for the four phases of the cell cycle, as well as for quiescence. Functions are assigned to some modifications in particular phases with information from the literature (black) and data from this study (red).

is likely associated with both reversible and irreversible cell cycle exit. Other nondividing states, such as differentiation of murine myogenic and neural lineages, also show increased levels of H4K20me3 (Biron *et al.*, 2004; Tsang *et al.*, 2010), and mass spectrometry analysis of differentiating embryonic stem cells showed a correlation between H4K20 methylation and loss of pluripotency (Phanstiel *et al.*, 2008). In our experiments, contact-inhibited and senescent fibroblasts had a similar H4K20 profile despite the fact that senescent and quiescent cells have very different chromatin structures (Rai and Adams, 2012). Recent analysis of senescence-associated heterochromatin foci, however, demonstrate that these structures are not dependent on changes in the levels of repressive chromatin marks such as H3K9me3 (Chandra *et al.*, 2012; Chandra and Narita, 2013), making increases in H4K20 unlikely to drive chromatin changes associated with senescence. The aging process often involves cellular senescence within an organism, and H4K20me3 was found to increase in 450-d-old rat livers (Sarg *et al.*, 2002). H4K20me1 was shown to decrease in 12-mo-old mouse brains (Wang *et al.*, 2009), which could be indicative of a shift to H4K20me2 and H4K20me3. These studies further highlight the link between nondivision and increases in H4K20me2 and H4K20me3.

We discovered that overexpression of Suv4-20h1, the methyltransferase that creates the dimethylated form of H4K20 at the expense of the monomethylated form, caused cell cycle arrest in G_2. This phenotype could reflect an overabundance of dimethylated H4K20 or a relative depletion of monomethylated H4K20 (Supplemental Figure S4). Previous reports indicated that a lack of H4K20me1 caused by inactivation of PR-Set7 results in activation of a G_2/M checkpoint (Abbas *et al.*, 2010) and abnormal chromosomes during mitosis (Rice *et al.*, 2002; Oda *et al.*, 2009). The phenotypes associated with a lack of H4K20me1 could reflect the importance of H4K20me1 in chromatin condensation, as subunits of the condensin II complex and other proteins have been found to bind H4K20me1 and can induce chromatin condensation in vitro (Trojer *et al.*, 2007; Liu *et al.*, 2010). Further, H4K20me1 can recruit L3MBTL1, which preferentially binds monomethylated and dimethylated lysines and induces chromatin compaction to negatively regulate gene expression (Trojer *et al.*, 2007; Kalakonda *et al.*, 2008).

A reduction in Suv4-20h2 resulted in defects in both S-phase cell number and cell cycle exit. Knockdown cells cultured in the presence of full serum contained an increased fraction of cells in S phase compared with controls. Further, in response to serum starvation or contact inhibition, there were more S-phase cells in knockdown than control cell populations. Increased numbers of cells in S phase could result from cells progressing through S phase more slowly or cells being blocked in S phase. Recent reports suggest a role for H4K20 in origin licensing and specifically demonstrate binding of H4K20me3 to ORC components (Vermeulen *et al.*, 2011; Beck *et al.*, 2012). Therefore it is possible that a loss of H4K20me3 may interfere with normal origin firing and lead to defects in S-phase progression. Alternatively, the propensity to proliferate in cells in which Suv4-20h2 is knocked down may be due to a loss of H4K20me3 at critical regions of the genome, such as cell cycle regulatory genes. H4K20me3 deposition has been shown to be dependent on Rb (Gonzalo *et al.*, 2005), and loss of the modification may affect expression of E2F genes. We observed additional S-phase cells at the expense of G_1/G_0 cells, suggesting that cells are likely to be exiting G_1/G_0 and progressing into S phase faster.

Modifications of H4K20 may be functionally important for quiescence. Dimethylated H4K20 serves as a binding site for the DNA-damage recognition protein 53BP1 and thereby helps to mediate repair of double-strand breaks (Sanders *et al.*, 2004; Botuyan *et al.*, 2006). Mouse embryonic fibroblasts containing null alleles for the two Suv4-20h histone methyltransferases exhibit increased sensitivity to damaging stress as a result of inadequate double-strand break repair (Schotta *et al.*, 2008). Quiescent cells cannot engage in the high-fidelity DNA repair mechanism of homologous recombination because there are no sister chromosomes from which to perform homologous recombination (Blanpain *et al.*, 2011). Instead, they must rely on the error-prone pathway of nonhomologous end joining. Higher H4K20me2 levels in quiescent cells could help them to initiate DNA repair events, which might help to protect them from DNA damage.

H4K20me3, the mark most significantly enriched in quiescent chromatin, is colocalized with H3K9me3 at centromeres (Martens *et al.*, 2005), telomeres (Benetti *et al.*, 2007), and pericentric heterochromatin (Schotta *et al.*, 2004). The methyltransferase for H4K20me3 may be recruited to sites of H3K9me3 via interaction with the H3K9me3-binding protein Hp1 (Schotta *et al.*, 2004). Depletion of H4K20me3 by knockdown of Suv4-20h1 and Suv4-20h2 results in depletion of dimethyl and trimethylated H4K20, and chromosomes are less compactly organized, consistent with such a role for this modification. We did not detect significant changes in the levels of H3K9me3 between proliferating and quiescent cells, but with H4K20me3 constituting <2% of H4, we might not have detected such a small change in H3K9me3.

Loss of trimethylation at H4K20 is a common hallmark of human cancer (Fraga *et al.*, 2005; Pogribny *et al.*, 2006; Van Den Broeck *et al.*, 2008; Schneider *et al.*, 2011). In a large panel of cancer cells and matched tumors and normal tissue, histone H4 consistently exhibited decreased trimethylation in cells derived from tumors (Fraga *et al.*, 2005). In one study of bladder cancer, H4K20me3 levels decreased with increasing tumor grade (Schneider *et al.*, 2011). In lung tumors, an association was observed between low levels of H4K20me3 and decreased levels of Suv4-20h2 (Van Den Broeck *et al.*, 2008). Decreased expression of H4K20me3 could reflect the proliferative state of the tumor cells. Alternatively, lower levels of H4K20me3 could promote tumorigenesis by preventing the repression of genes that control cell cycle progression and thereby inhibiting formation of a proper out-of-cycle state. A better understanding of the changes in chromatin dynamics as cells enter, maintain, and exit a quiescent state is likely to provide important insights into the control of cellular proliferation and how this process is altered in developmental abnormalities, aging, and cancer.

MATERIALS AND METHODS

Cell culture

Primary human foreskin fibroblasts (HFFs) were isolated from donor foreskins as previously described (Legesse-Miller *et al.*, 2009). All experiments were performed in cells with a passage number of <13. Cells were cultured in DMEM (Invitrogen, Carlsbad, CA) with 10% fetal bovine serum unless otherwise indicated. Proliferating cells were plated at 50% confluence and harvested after 24 h to avoid contact inhibition. Contact-inhibited cells were plated at 50% confluence and incubated for the indicated number of days with medium changes every 3 d. Cells used for histone analysis were scraped in phosphate-buffered saline (PBS) from tissue culture plates and flash frozen in liquid nitrogen.

Cell synchronization

HFFs were plated at 30–40% confluence and maintained in a 37°C incubator for 16 h. Cells were initially washed 2X with PBS and serum-starved for 24 h in DMEM with 0.1% fetal bovine serum (FBS) to synchronize them in G_1. Cells were then washed 2× with PBS and incubated with DMEM + 10% FBS + 2 mM hydroxyurea to release them from serum starvation–induced arrest and block them at the G_1/S transition. After incubation for 18 h, cells were washed 2× with PBS, and fresh DMEM with 10% FBS was added to allow a synchronized exit into other cell cycle phases. Cells were harvested at 3 h (S phase), 6.5 h (G_2/M phases), and 12 h (G_1 phase).

Senescence model

A total of 5×10^6 Phoenix cells was transfected with 5 μg of Ampho helper plasmid (Imgenex, San Diego, CA) and 5 μg of either pBABE or pBABE-Ras^{G12V} using Arrest-In (Open Biosystems, Huntsville, AL). Viral supernatant was collected 48 h posttransfection and filtered with a 0.45-μm filter. Cycling human fibroblasts were infected for 24 h with viral supernatant plus Polybrene at 2.6 μg/ml. Cells were selected for 48 h in DMEM + 10% FBS + 2 μg/ml puromycin. After selection, cells were passaged approximately three times until cell division ceased. Cells were fixed between 1 and 14 d after cell cycle arrest and stained with X-gal for 8 h to visualize β-galactosidase–positive cells.

Flow cytometry

HFFs were removed from plates with PBS + 0.05% trypsin-EDTA. For propidium iodide staining, cells were fixed and permeabilized by adding one volume of PBS to two volumes of 100% ethanol and stored at 4°C for >24 h. Ethanol was removed, and cells were incubated with propidium iodide (PI; 40 μg/ml; EMD Chemicals, Gibbstown, NJ) and RNase A (200 μg/ml; Roche, Basel, Switzerland) in PBS for 1 h in the dark. For Click-iT analysis, cells were incubated for 2 h in 10 mM EdU. Cells were pelleted, fixed with 4% paraformaldehyde, and treated with Alexa 488 azide (Invitrogen). DNA was stained with 4′,6-diamidino-2-phenylindole (DAPI). All cells were analyzed with a FACScaliber flow cytometer (BD Biosciences, San Jose, CA). At least 20,000 cells were analyzed per sample. The software FlowJo (version 8.8.2, Watson algorithm) was used to estimate the fraction of cells in G_1, S, and G_2/M for PI-stained cells. Paired *t* tests were used to determine whether the fraction of cells in different phases of the cell cycle were significantly different in knockdown cells and controls.

Histone isolation and preparation for MS

Histones were purified using acid extraction as previously described (Shechter *et al.*, 2007). Briefly, cell pellets were thawed and resuspended in 10 volumes (for every volume of cell pellet) of nuclear isolation buffer (15 mM Tris-HCl at pH 7.5; 60 mM KCl; 15 mM NaCl; 5 mM $MgCl_2$; 1 mM $CaCl_2$; 250 mM sucrose; 1 mM DTT; 5 μM microcystin; 500 μM 4-(2-aminoethyl) benzenesulfonyl fluoride hydrochloride; 10 mM sodium butyrate) with 10% NP-40 and incubated for 5 min. Nuclei were washed 2× with nuclear isolation buffer lacking NP-40 and then mixed with five volumes (for every volume of nuclei) of 0.4 N H_2SO_4 and incubated for 3–4 h at 4°C. Histones were precipitated with trichloroacetic acid and washed once with acetone containing 0.1% HCl, followed by two washes with 100% acetone. Histones were air dried overnight and resuspended in H_2O. Histones were processed using methods previously described (Plazas-Mayorca *et al.*, 2009). A solution containing 100 μg of purified histones was reduced to 40 μl using a vacuum concentrator and mixed with 20 μl of 3:1 anhydrous isopropanol to propionic anhydride

(Sigma-Aldrich, Basel, Switzerland). The mixture was incubated at 37°C for 15 min and reduced back to 40 µl, constituting one round of "propionylation." The process was repeated one additional time, and the solution was then reduced to near dryness. Histones were resuspended in 100 µl of 100 mM ammonium bicarbonate (pH 8.0) and digested with trypsin (Promega, Madison, WI) at a ratio of 1:50 trypsin to histones for 6–8 h at 37°C, followed by quenching of the reaction by acidifying with glacial acetic acid (to pH <5) and freezing at –80°C. Two additional rounds of propionylation were performed to modify the newly exposed N-termini of histone peptides. To quantify two samples in the mass spectrometer, one sample was modified by propionic anhydride containing deuterium instead of hydrogen (Cambridge Isotope Laboratories, Andover, MA), causing a mass shift of +5 Da. Histone peptides from two samples were then mixed and purified of salts with C_{18} STAGE-Tips constructed as described previously (Rappsilber *et al.*, 2003).

Nano-LC-MS/MS

Histones were separated by reversed-phase high-performance liquid chromatography (HPLC) on an Agilent 1200 series HPLC system (Agilent, Santa Clara, CA) using a 75-µm–inner diameter fused silica column packed with 10–15 cm of 5-µm C_{18} (Michrom, Auburn, CA). A gradient of 0.7–30% buffer B in buffer A (buffer A, 0.1 M acetic acid; buffer B, 95% acetonitrile in 0.1 M acetic acid) for 35 min followed by 30–98% buffer B for 30 min was used to elute peptides, which were ionized via electrospray ionization. Peptides were analyzed in a LTQ-Orbitrap mass spectrometer (ThermoFisher Scientific, San Jose, CA). Full scans of m/z = 290–1000 with a resolution of 30,000 were measured in the Orbitrap. Collision-induced dissociation was used to fragment ions corresponding to isobaric acetylated peptides (H3K9ac or K14ac [528.296, z = +2] and H3K18ac or K23ac [570.841, z = +2]) in segments where those peptides elute; in other segments data-dependent fragmentation was performed on the seven most intense ions. Extracted ion chromatograms from Orbitrap data were integrated to yield intensity values for all histone peptides of interest. The values for all modified forms of a particular peptide were used to find the relative abundance of individual modified forms for that peptide.

Dual-color fluorescence in situ hybridization

Cells were harvested and incubated at 37°C for 30 min in 0.59% KCl. Cells were fixed in ice-cold methanol:acetic acid at a 3:1 ratio and spread on glass slides. Slides were prepared for FISH using fluorescently labeled probes specific for the arms of chromosome 16 (16q22, red; 16p13, green) according to the manufacturer's instructions (LPH 022; Cytocell, Cambridge, United Kingdom). Coverslips were mounted, and DNA was detected with 0.2 µg/ml DAPI/antifade solution (Cytocell). Fluorescence images were captured with an Orca AG cooled charge-coupled device camera (Hamamatsu, Hamamatsu, Japan) mounted on a Nikon TI (Melville, NY)/Yokagawa (Tokyo, Japan) CSU-10 spinning disk confocal microscope with a 100×, 1.4 numerical aperture objective. A series of 0.25-µm optical sections was collected in the z-axis for each channel (DAPI, fluorescein, and Texas red). Intrachromosome distances under each condition were measured with SlideBook analysis software (SlideBook, Denver, CO). Approximately 30–100 cells were used to measure intrachromosome distances for each condition, and three biological replicates were scored.

Immunoblotting and immunofluorescence

We separated 10 µg of acid-extracted histones on a 15% polyacrylamide gel. Primary rabbit anti-H4K20me3 (Novus Biologicals, Littleton, CO) was incubated for 16 h at 4°C. A secondary antibody was incubated for 1 h at room temperature at 1:10,000 dilution, and the membrane was exposed using an enhanced chemiluminescence detection kit. For antibody testing, modified peptides (AnaSpec, Fremont, CA) were spotted onto a polyvinylidene fluoride membrane. Primary and secondary conditions were identical to those described earlier except that streptavidin–horseradish peroxidase (PerkinElmer, Waltham, MA) was used instead of a secondary antibody. For immunofluorescence, cells were grown on glass slides (EZ slide; EMD Millipore, Billerica, MA) and fixed using 4% formaldehyde for 15 min. After permeabilization for 20 min with methanol, cells were treated with blocking buffer and antibodies as described for Western blotting. Anti–rabbit-488 was used for detection of antibodies, and cells were stained with DAPI at 1 µg/ml to visualize the nucleus.

Overexpression/knockdown

The CDS of Suv4-20h1 (variant 1) was PCR amplified from human cDNA (forward, 5′-*CCCGGGttaattaaATGAAGTGGTTGGGAGAA-TCCAAGA*-3′; reverse, 5′-*CCCGGGggatccTTAGGCATTAAGCCT-TAAAGACTGA*-3′) and cloned into retroviral vector pQCXIP using *Pac*I and *Bam*HI restriction sites. Vectors that express short hairpin RNAs (shRNAs) against Suv4-20h1 (*GTTTGTGTCAACTGGTCGA-GATACAGCAT*) and Suv4-20h2 (*CGACCTGGATGTCGGCGGT-GAAGAGCTGT*) were purchased from OriGene (Rockville, MD). Virus was generated and collected as described (senescence model). For overexpression, fibroblasts were transduced with pQCXIP– or pQCXIP-Suv4-20h1–derived virus and selected for 48 h with 2 µg/ml puromycin. For the Suv4-20h1/h2 knockdowns, an shRNA against green fluorescent protein (puromycin resistance gene) and a scrambled shRNA (blasticidin resistance gene) were used as controls. Both control viruses or viruses derived from shRNAs to Suv4-20h1/h2 were used to coinfect fibroblasts. Infected cells were selected with 2 µg/ml puromycin and 30 µg/ml blasticidin for 5 d. Cells expressing shRNAs were passaged three or more times to sufficiently reduce histone modification levels before analysis. Cells expressing Suv4-20h1 were maintained for 24 h without selection media and analyzed. siRNAs were purchased from Thermo Scientific (Lafayette, CO) as siGENOME SMARTpools targeting Suv4-20h1 and Suv4-20h2. We transfected 100 nM of each siRNA pool or 200 nM of control siRNAs into HFFs using Oligofectamine (Invitrogen, Carlsbad, CA). Cells were expanded for 48 h, transfected again, and either analyzed 24 h later as proliferating cells or serum starved for 24 h and then analyzed.

ACKNOWLEDGMENTS

We thank Eric Neeley (Novus Biologicals) for providing reagents and all of the members of the Coller and Garcia laboratories for helpful discussions. A.L.M. is supported in part by an American Cancer Society Postdoctoral Fellowship. A.L.M. and N.J.D. are supported by National Institutes of Health Grant R01 CA155202. B.A.G. is supported by a National Science Foundation Early Faculty CAREER award, National Science Foundation Grant CBET-0941143, and a grant supported by Award DP2OD007447 from the Office of the Director, National Institutes of Health. H.A.C. is supported by National Institute of General Medical Sciences Center of Excellence Grant P50 GM071508, the Cancer Institute of New Jersey, the New Jersey Commission on Cancer Research, National Cancer Institute 1RC1 CA147961-01, a Focused Funding Grant from the Johnson & Johnson Foundation, and National Institutes of Health/National Institute of General Medical Sciences Grants 1R01 GM081686 and 1R01 GM086465. H.A.C. was a Milton E. Cassel Scholar of the Rita Allen Foundation.

REFERENCES

Abbas T, Shibata E, Park J, Jha S, Karnani N, Dutta A (2010). CRL4(Cdt2) regulates cell proliferation and histone gene expression by targeting PR-Set7/Set8 for degradation. Mol Cell 40, 9–21.

Baxter J *et al.* (2004). Histone hypomethylation is an indicator of epigenetic plasticity in quiescent lymphocytes. EMBO J 23, 4462–4472.

Beck DB, Burton A, Oda H, Ziegler-Birling C, Torres-Padilla ME, Reinberg D (2012). The role of PR-Set7 in replication licensing depends on Suv4-20h. Genes Dev 26, 2580–2589.

Benetti R, Gonzalo S, Jaco I, Schotta G, Klatt P, Jenuwein T, Blasco MA (2007). Suv4–20h deficiency results in telomere elongation and derepression of telomere recombination. J Cell Biol 178, 925–936.

Biron VL, McManus KJ, Hu N, Hendzel MJ, Underhill DA (2004). Distinct dynamics and distribution of histone methyl-lysine derivatives in mouse development. Dev Biol 276, 337–351.

Blanpain C, Mohrin M, Sotiropoulou PA, Passegue E (2011). DNA-damage response in tissue-specific and cancer stem cells. Cell Stem Cell 8, 16–29.

Botuyan MV, Lee J, Ward IM, Kim JE, Thompson JR, Chen J, Mer G (2006). Structural basis for the methylation state-specific recognition of histone H4-K20 by 53BP1 and Crb2 in DNA repair. Cell 127, 1361–1373.

Bystricky K, Heun P, Gehlen L, Langowski J, Gasser SM (2004). Long-range compaction and flexibility of interphase chromatin in budding yeast analyzed by high-resolution imaging techniques. Proc Natl Acad Sci USA 101, 16495–16500.

Caretti G, Di Padova M, Micales B, Lyons GE, Sartorelli V (2004). The Polycomb Ezh2 methyltransferase regulates muscle gene expression and skeletal muscle differentiation. Genes Dev 18, 2627–2638.

Centore RC, Havens CG, Manning AL, Li JM, Flynn RL, Tse A, Jin J, Dyson NJ, Walter JC, Zou L (2010). CRL4(Cdt2)-mediated destruction of the histone methyltransferase Set8 prevents premature chromatin compaction in S phase. Mol Cell 40, 22–33.

Chambeyron S, Bickmore WA (2004). Chromatin decondensation and nuclear reorganization of the HoxB locus upon induction of transcription. Genes Dev 18, 1119–1130.

Chandra T *et al.* (2012). Independence of repressive histone marks and chromatin compaction during senescent heterochromatic layer formation. Mol Cell 47, 203–214.

Chandra T, Narita M (2013). High-order chromatin structure and the epigenome in SAHFs. Nucleus 4, 23–28.

Chiu N, Baserga R (1975). Changes in template activity and structure of nuclei from WI-38 cells in the prereplicative phase. Biochemistry 14, 3126–3132.

Coller HA, Sang L, Roberts JM (2006). A new description of cellular quiescence. PLoS Biol 4, e83.

Coppock DL, Kopman C, Scandalis S, Gilleran S (1993). Preferential gene expression in quiescent human lung fibroblasts. Cell Growth Differ 4, 483–493.

Dardick I, Sinnott NM, Hall R, Bajenko-Carr TA, Setterfield G (1983). Nuclear morphology and morphometry of B-lymphocyte transformation. Implications for follicular center cell lymphomas. Am J Pathol 111, 35–49.

Evertts AG, Zee BM, Dimaggio PA, Gonzales-Cope M, Coller HA, Garcia BA (2013). Quantitative dynamics of the link between cellular metabolism and histone acetylation. J Biol Chem 288, 12142–12151.

Fang J, Feng Q, Ketel CS, Wang H, Cao R, Xia L, Erdjument-Bromage H, Tempst P, Simon JA, Zhang Y (2002). Purification and functional characterization of SET8, a nucleosomal histone H4-lysine 20-specific methyltransferase. Curr Biol 12, 1086–1099.

Fraga MF *et al.* (2005). Loss of acetylation at Lys16 and trimethylation at Lys20 of histone H4 is a common hallmark of human cancer. Nat Genet 37, 391–400.

Gonzalo S *et al.* (2005). Role of the RB1 family in stabilizing histone methylation at constitutive heterochromatin. Nat Cell Biol 7, 420–428.

Grigoryev SA, Nikitina T, Pehrson JR, Singh PB, Woodcock CL (2004). Dynamic relocation of epigenetic chromatin markers reveals an active role of constitutive heterochromatin in the transition from proliferation to quiescence. J Cell Sci 117, 6153–6162.

Jaehning JA, Stewart CC, Roeder RG (1975). DNA-dependent RNA polymerase levels during the response of human peripheral lymphocytes to phytohemagglutinin. Cell 4, 51–57.

Jenuwein T, Allis CD (2001). Translating the histone code. Science 293, 1074–1080.

Jorgensen S, Elvers I, Trelle MB, Menzel T, Eskildsen M, Jensen ON, Helleday T, Helin K, Sorensen CS (2007). The histone methyltransferase SET8 is required for S-phase progression. J Cell Biol 179, 1337–1345.

Jorgensen S *et al.* (2011). SET8 is degraded via PCNA-coupled CRL4(CDT2) ubiquitylation in S phase and after UV irradiation. J Cell Biol 192, 43–54.

Julien E, Herr W (2004). A switch in mitotic histone H4 lysine 20 methylation status is linked to M phase defects upon loss of HCF-1. Mol Cell 14, 713–725.

Kalakonda N *et al.* (2008). Histone H4 lysine 20 monomethylation promotes transcriptional repression by L3MBTL1. Oncogene 27, 4293–4304.

Kim W, Kim R, Park G, Park JW, Kim JE (2012). Deficiency of H3K79 histone methyltransferase Dot1-like protein (DOT1L) inhibits cell proliferation. J Biol Chem 287, 5588–5599.

Kourmouli N *et al.* (2004). Heterochromatin and tri-methylated lysine 20 of histone H4 in animals. J Cell Sci 117, 2491–2501.

Legesse-Miller A, Elemento O, Pfau SJ, Forman JJ, Tavazoie S, Coller HA (2009). let-7 Overexpression leads to an increased fraction of cells in G2/M, direct down-regulation of Cdc34, and stabilization of Wee1 kinase in primary fibroblasts. J Biol Chem 284, 6605–6609.

Lemons JM *et al.* (2010). Quiescent fibroblasts exhibit high metabolic activity. PLoS Biol 8, e1000514.

Liu W *et al.* (2010). PHF8 mediates histone H4 lysine 20 demethylation events involved in cell cycle progression. Nature 466, 508–512.

Lu X, Simon MD, Chodaparambil JV, Hansen JC, Shokat KM, Luger K (2008). The effect of H3K79 dimethylation and H4K20 trimethylation on nucleosome and chromatin structure. Nat Struct Mol Biol 15, 1122–1124.

Mal AK (2006). Histone methyltransferase Suv39h1 represses MyoD-stimulated myogenic differentiation. EMBO J 25, 3323–3334.

Marion RM, Schotta G, Ortega S, Blasco MA (2011). Suv4-20h abrogation enhances telomere elongation during reprogramming and confers a higher tumorigenic potential to iPS cells. PLoS One 6, e25680.

Martens JH, O'Sullivan RJ, Braunschweig U, Opravil S, Radolf M, Steinlein P, Jenuwein T (2005). The profile of repeat-associated histone lysine methylation states in the mouse epigenome. EMBO J 24, 800–812.

Nishioka K *et al.* (2002). PR-Set7 is a nucleosome-specific methyltransferase that modifies lysine 20 of histone H4 and is associated with silent chromatin. Mol Cell 9, 1201–1213.

Oda H, Okamoto I, Murphy N, Chu J, Price SM, Shen MM, Torres-Padilla ME, Heard E, Reinberg D (2009). Monomethylation of histone H4-lysine 20 is involved in chromosome structure and stability and is essential for mouse development. Mol Cell Biol 29, 2278–2295.

Pardee AB (1974). A restriction point for control of normal animal cell proliferation. Proc Natl Acad Sci USA 71, 1286–1290.

Pesavento JJ, Yang H, Kelleher NL, Mizzen CA (2008). Certain and progressive methylation of histone H4 at lysine 20 during the cell cycle. Mol Cell Biol 28, 468–486.

Phalke S, Nickel O, Walluscheck D, Hortig F, Onorati MC, Reuter G (2009). Retrotransposon silencing and telomere integrity in somatic cells of *Drosophila* depends on the cytosine-5 methyltransferase DNMT2. Nat Genet 41, 696–702.

Phanstiel D, Brumbaugh J, Berggren WT, Conard K, Feng X, Levenstein ME, McAlister GC, Thomson JA, Coon JJ (2008). Mass spectrometry identifies and quantifies 74 unique histone H4 isoforms in differentiating human embryonic stem cells. Proc Natl Acad Sci USA 105, 4093–4098.

Plazas-Mayorca MD, Zee BM, Young NL, Fingerman IM, LeRoy G, Briggs SD, Garcia BA (2009). One-pot shotgun quantitative mass spectrometry characterization of histones. J Proteome Res 8, 5367–5374.

Pogribny IP, Ross SA, Tryndyak VP, Pogribna M, Poirier LA, Karpinets TV (2006). Histone H3 lysine 9 and H4 lysine 20 trimethylation and the expression of Suv4-20h2 and Suv-39h1 histone methyltransferases in hepatocarcinogenesis induced by methyl deficiency in rats. Carcinogenesis 27, 1180–1186.

Pollina EA, Legesse-Miller A, Haley EM, Goodpaster T, Randolph-Habecker J, Coller HA (2008). Regulating the angiogenic balance in tissues. Cell Cycle 7, 2056–2070.

Rai TS, Adams PD (2012). Lessons from senescence: chromatin maintenance in non-proliferating cells. Biochim Biophys Acta 1819, 322–331.

Rappsilber J, Ishihama Y, Mann M (2003). Stop and go extraction tips for matrix-assisted laser desorption/ionization, nanoelectrospray, and LC/MS sample pretreatment in proteomics. Anal Chem 75, 663–670.

Rawlings JS, Gatzka M, Thomas PG, Ihle JN (2011). Chromatin condensation via the condensin II complex is required for peripheral T-cell quiescence. EMBO J 30, 263–276.

Rice JC, Nishioka K, Sarma K, Steward R, Reinberg D, Allis CD (2002). Mitotic-specific methylation of histone H4 Lys 20 follows increased PR-Set7 expression and its localization to mitotic chromosomes. Genes Dev 16, 2225–2230.

Sanders SL, Portoso M, Mata J, Bahler J, Allshire RC, Kouzarides T (2004). Methylation of histone H4 lysine 20 controls recruitment of Crb2 to sites of DNA damage. Cell 119, 603–614.
Sarg B, Koutzamani E, Helliger W, Rundquist I, Lindner HH (2002). Postsynthetic trimethylation of histone H4 at lysine 20 in mammalian tissues is associated with aging. J Biol Chem 277, 39195–39201.
Schneider AC, Heukamp LC, Rogenhofer S, Fechner G, Bastian PJ, von Ruecker A, Muller SC, Ellinger J (2011). Global histone H4K20 trimethylation predicts cancer-specific survival in patients with muscle-invasive bladder cancer. BJU Int 108, E290–E296.
Schneider C, King RM, Philipson L (1988). Genes specifically expressed at growth arrest of mammalian cells. Cell 54, 787–793.
Schotta G, Lachner M, Sarma K, Ebert A, Sengupta R, Reuter G, Reinberg D, Jenuwein T (2004). A silencing pathway to induce H3-K9 and H4-K20 trimethylation at constitutive heterochromatin. Genes Dev 18, 1251–1262.
Schotta G *et al*. (2008). A chromatin-wide transition to H4K20 monomethylation impairs genome integrity and programmed DNA rearrangements in the mouse. Genes Dev 22, 2048–2061.
Schubeler D, Francastel C, Cimbora DM, Reik A, Martin DI, Groudine M (2000). Nuclear localization and histone acetylation: a pathway for chromatin opening and transcriptional activation of the human beta-globin locus. Genes Dev 14, 940–950.
Schulze JM, Jackson J, Nakanishi S, Gardner JM, Hentrich T, Haug J, Johnston M, Jaspersen SL, Kobor MS, Shilatifard A (2009). Linking cell cycle to histone modifications: SBF and H2B monoubiquitination machinery and cell-cycle regulation of H3K79 dimethylation. Mol Cell 35, 626–641.
Setterfield G, Hall R, Bladon T, Little J, Kaplan JG (1983). Changes in structure and composition of lymphocyte nuclei during mitogenic stimulation. J Ultrastruct Res 82, 264–282.
Shechter D, Dormann HL, Allis CD, Hake SB (2007). Extraction, purification and analysis of histones. Nat Protoc 2, 1445–1457.
Tokuyasu K, Madden SC, Zeldis LJ (1968). Fine structural alterations of interphase nuclei of lymphocytes stimulated to growth activity in vitro. J Cell Biol 39, 630–660.
Trojer P *et al*. (2007). L3MBTL1, a histone-methylation-dependent chromatin lock. Cell 129, 915–928.
Tsang LW, Hu N, Underhill DA (2010). Comparative analyses of SUV420H1 isoforms and SUV420H2 reveal differences in their cellular localization and effects on myogenic differentiation. PLoS One 5, e14447.
Van Den Broeck A, Brambilla E, Moro-Sibilot D, Lantuejoul S, Brambilla C, Eymin B, Khochbin S, Gazzeri S (2008). Loss of histone H4K20 trimethylation occurs in preneoplasia and influences prognosis of non-small cell lung cancer. Clin Cancer Res 14, 7237–7245.
Venezia TA, Merchant AA, Ramos CA, Whitehouse NL, Young AS, Shaw CA, Goodell MA (2004). Molecular signatures of proliferation and quiescence in hematopoietic stem cells. PLoS Biol 2, e301.
Vermeulen M *et al*. (2011). Quantitative interaction proteomics and genome-wide profiling of epigenetic histone marks and their readers. Cell 142, 967–980.
Wang CM, Tsai SN, Yew TW, Kwan YW, Ngai SM (2009). Identification of histone methylation multiplicities patterns in the brain of senescence-accelerated prone mouse 8. Biogerontology 11, 87–102.
Wu S, Wang W, Kong X, Congdon LM, Yokomori K, Kirschner MW, Rice JC (2010). Dynamic regulation of the PR-Set7 histone methyltransferase is required for normal cell cycle progression. Genes Dev 24, 2531–2542.
Yang H, Pesavento JJ, Starnes TW, Cryderman DE, Wallrath LL, Kelleher NL, Mizzen CA (2008). Preferential dimethylation of histone H4 lysine 20 by Suv4-20. J Biol Chem 283, 12085–12092.
Young NL, DiMaggio PA, Plazas-Mayorca MD, Baliban RC, Floudas CA, Garcia BA (2009). High throughput characterization of combinatorial histone codes. Mol Cell Proteomics 8, 2266–2284.
Zee BM, Britton LM, Wolle D, Haberman DM, Garcia BA (2012). Origins and formation of histone methylation across the human cell cycle. Mol Cell Biol 32, 2503–2514.
Zhang CL, McKinsey TA, Olson EN (2002). Association of class II histone deacetylases with heterochromatin protein 1: potential role for histone methylation in control of muscle differentiation. Mol Cell Biol 22, 7302–7312.